

Winds Can “Blow Up” AGN Accretion Disk Sizes

MOUYUAN SUN,^{1,2} YONGQUAN XUE,^{1,2} JONATHAN R. TRUMP,³ AND WEI-MIN GU⁴

¹CAS Key Laboratory for Research in Galaxies and Cosmology, Department of Astronomy, University of Science and Technology of China, Hefei 230026, China; ericsun@ustc.edu.cn; xuey@ustc.edu.cn

²School of Astronomy and Space Science, University of Science and Technology of China, Hefei 230026, China

³Department of Physics, University of Connecticut, Storrs, CT 06269, USA

⁴Department of Astronomy, Xiamen University, Xiamen, Fujian 361005, China

(Revised Draft: May 26, 2022)

ABSTRACT

Recent multi-band variability studies have revealed that active galactic nucleus (AGN) accretion disk sizes are generally larger than the predictions of the classical thin disk by a factor of $2 \sim 3$. This hints at some missing key ingredient in the classical thin disk theory, which is likely wind as we propose. For a given bolometric luminosity, in the outer part of an accretion disk, the effective temperature in the wind case is higher than that in the no-wind one.; meanwhile, the radial temperature profile of the wind case is flatter than the no-wind one. In presence of winds, for a given band, blackbody emission from large radii can contribute more to the observed luminosity than the no-wind case. Therefore, the disk sizes of the wind case can be larger than those of the no-wind case. We demonstrate that a model with the accretion rate scaling as $\dot{M}_0(R/R_S)^\beta$ (i.e., the accretion rate declines with decreasing radius due to winds) can match both the inter-band time lags and the spectral energy distribution of NGC 5548. Our model can also explain the inter-band time lags of other sources. Therefore, our model can help decipher current and future continuum reverberation mapping observations.

Keywords: black hole physics—galaxies: active—galaxies: individual (NGC 5548)

1. INTRODUCTION

The cross correlation between two light curves of active galactic nucleus (AGN) continuum emission can provide model-independent constraints on the accretion disk sizes. The inter-band correlations might be caused by X-ray (e.g., Krolik et al. 1991) or far-ultraviolet (FUV) reprocessing (Gardner & Done 2017). According to the reprocessing scenario, X-ray or FUV emission acts as an external energy source (in addition to the internal viscous dissipation) and heats the outer accretion disk. As a result, emission at longer wavelengths (e.g., UV, optical and infrared (IR)) varies in response to X-ray or FUV variations (i.e., the “driving light curves”) after a light-travel time delay (i.e., continuum reverberation mapping). Therefore, the inter-band time lags can probe the accretion disk sizes. However, the observed inter-band time lags are incompatible with the classical thin disk theory of Shakura & Sunyaev (1973). Indeed, the observed accretion disk sizes are $2 \sim 3$ times larger than the theoretical expectations (e.g., Edelson et al. 2015; Fausnaugh et al. 2016; Edelson et al. 2017; Jiang et al. 2017; McHardy et al. 2017; Starkey et al. 2017). Accretion disk sizes inferred from microlensing observations of quasars are also larger than expected (e.g., Morgan et al. 2010). These observational results indicate that some key ingredient is missing in the classical thin disk theory.

Several scenarios have been proposed to explain the larger-than-expected accretion disk sizes. For instance, Dexter & Agol (2011) suggest that an inhomogeneous accretion disk with temperature fluctuations can explain the microlensing results. With some further modifications, this model can also explain the timescale-dependent color variations (Cai et al. 2016; Zhu et al. 2017) and accretion disk sizes (Cai et al. 2018). Gardner & Done (2017) argue that the observed inter-band time lags are not the simple light-travel timescales but correspond to other physical timescales (e.g., the dynamical or thermal timescales). It is also speculated that the larger-than-expected time lags are caused by contribution of diffuse continuum emission from broad emission line (BEL) region (Cackett et al. 2017; McHardy et al. 2017). Last but not least, a non-blackbody disk due to electron scattering in the disk atmosphere can be used to explain the observed time lags; however, such a disk emits too much soft X-ray emission (Hall et al. 2018).

Here, we propose an alternative model to explain the larger-than-expected accretion disk sizes: an accretion disk suffers from significant winds. To emit the same bolometric luminosity (L_{bol}), in the outer part, the effective temperature of the disk with winds is higher than the no-wind one. In presence of winds, the radial temperature profile is flatter than the classical $T(R) \propto R^{-3/4}$ law. As a result, for a given band, blackbody emission from large radii can con-

tribute significantly to the total luminosity. Therefore, the accretion disk sizes inferred from inter-band time lags are larger than those of the classical disk model.

This work is formatted as follows. In Section 2, we explain our model in detail and explore the inter-band time lags of NGC 5548. We discuss our results in Section 3. We adopt a flat Λ CDM cosmology with $h_0 = 0.7$ and $\Omega_M = 0.3$.

2. THIN DISK WITH WINDS

2.1. General arguments

We consider that the thin disk suffers from significant winds with a radius-dependent mass rate, i.e., \dot{M} is a function of radius (R). The exact form of \dot{M} is not well known for thin disk. According to some magnetically driven wind models (e.g., Blandford & Payne 1982; Cao & Spruit 2013) and numerical simulations of hot accretion flows (e.g., Yuan et al. 2012a), \dot{M} can be expressed in a self-similar form,

$$\dot{M} = \dot{M}_0 r^\beta, \quad (1)$$

where the dimensionless parameter β denotes the strength of winds (without winds, $\beta = 0$); $r = R/R_S$ is the radial distance (R) to the central supermassive black hole (SMBH) in units of the Schwarzschild radius ($R_S = 2GM_{\text{BH}}/c^2$, where G , M_{BH} and c are the gravitational constant, black hole mass and speed of light, respectively); and \dot{M}_0 is a normalization factor (i.e., $\dot{M}_0 r_{\text{in}}^\beta$ is the accretion rate at the innermost stable circular orbit (ISCO), r_{in}). The disk emits multi-temperature black-body emission. The gravitational energy converted into the observed bolometric luminosity is

$$L_{\text{bol}} = \int_{r_{\text{out}}}^{r_{\text{in}}} -\frac{GM_{\text{BH}}\dot{M}}{2(rR_S)^2} d(rR_S) = \frac{\dot{M}_0 c^2}{4(1-\beta)r_{\text{in}}^{1-\beta}}, \quad (2)$$

where $r_{\text{in}} = 3$ for a non-spinning Schwarzschild black hole, and $r_{\text{out}} (\gg r_{\text{in}})$ is the outer boundary of the accretion disk (which is likely determined by the self-gravity radius; the self gravity dominates over the gravity of SMBH beyond this radius). For simplicity, we ignore the $1 - \sqrt{3r_{\text{in}}/r}$ term or relativistic effects. Such corrections are unimportant for UV-optical-IR emission regions. The local effective temperature of the disk is

$$T_{\text{eff}} = \left(\frac{3GM_{\text{BH}}\dot{M}_0}{8\pi\sigma R_S^3} \right)^{\frac{1}{4}} r^{\frac{\beta-3}{4}}, \quad (3)$$

where σ is the Stefan-Boltzmann constant. In Figure 1, we show the temperature profile for the no-wind and the wind with $\beta = 0.3$ cases. \dot{M}_0 is chosen such that the two cases have the same L_{bol} . The temperature profile of the wind case is flatter than that of the no-wind case. In addition, in the outer disk ($r > 10$), the effective temperature of the wind case is also higher than that of the no-wind case.

For a given wavelength λ , we can define a characteristic radius by setting $k_B T_{\text{eff}} = hc/\lambda$, that is,

$$R(\lambda) = \left\{ \frac{hc}{k_B \lambda} \left(\frac{8\pi\sigma R_S^3}{3GM_{\text{BH}}\dot{M}_0} \right)^{\frac{1}{4}} \right\}^{\frac{4}{\beta-3}}, \quad (4)$$

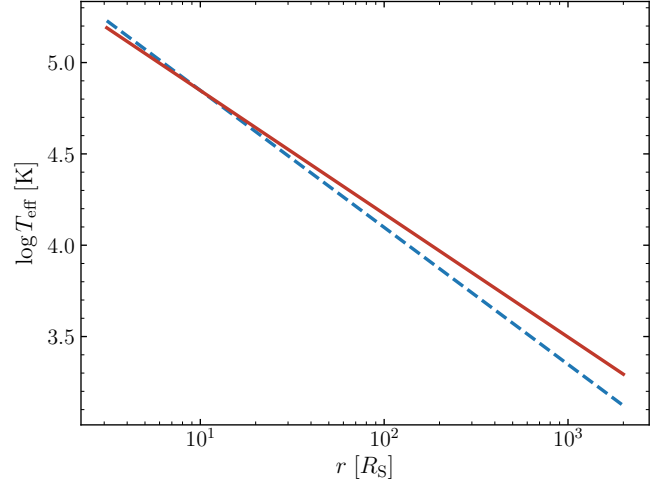


Figure 1. The radial distribution of effective temperature (T_{eff}) for cases with the wind parameter $\beta = 0.3$ (solid line) and $\beta = 0$ (i.e., no wind; dashed line), respectively. The two disks emit the same bolometric luminosity (i.e., $L_{\text{bol}} = 0.1L_{\text{Edd}}$; M_{BH} is $8 \times 10^7 M_{\odot}$). At outer radii (i.e., $r > 10$), the effective temperature T_{eff} for the wind case is larger than that for the no-wind case.

where h and k_B are the Planck constant and the Boltzmann constant, respectively. In reverberation mapping observations, the measured sizes are not $R(\lambda)$ but close to the flux-weighted radius (Fausnaugh et al. 2016) if the response function is proportional to flux. For the face-on case,

$$R_{\text{fl}}(\lambda) = \frac{\int_{r_{\text{in}}}^{r_{\text{out}}} \pi B(\lambda) (rR_S)^2 dr}{\int_{r_{\text{in}}}^{r_{\text{out}}} \pi B(\lambda) r R_S dr}, \quad (5)$$

where $B(\lambda)$ is the Planck function. It can be proven that, if $h\nu/k_B T_{\text{eff}}(r_{\text{out}}) \gg 1$ and $h\nu/k_B T_{\text{eff}}(r_{\text{in}}) \ll 1$ (e.g., the optical bands), the ratio $X = R_{\text{fl}}/R_{\lambda}$ is

$$X \cong \frac{\Gamma(\frac{12}{3-\beta})\zeta(\frac{12}{3-\beta})}{\Gamma(\frac{8}{3-\beta})\zeta(\frac{8}{3-\beta})}, \quad (6)$$

where $\zeta(x)$ and $\Gamma(x)$ denote the Riemann-zeta function and the Gamma function, respectively; otherwise (e.g., for the near-IR bands), Eq. 6 overestimates X . It is clear that X increases with β (Figure 2).¹ The results from Figures 1 & 2 suggest that the size of emission region for a given band increases with β .

2.2. NGC 5548 as a test case

To compare our model with the observed inter-band time lags of NGC 5548, we model a thin disk with winds; the physical parameters are $M_{\text{BH}} = 8 \times 10^7 M_{\odot}$ (Bentz et al. 2010), the inclination angle $i = \pi/4$ and the redshift

¹ The disk sizes also change with inclination angle, (see Figure 2 of Cackett et al. 2007).

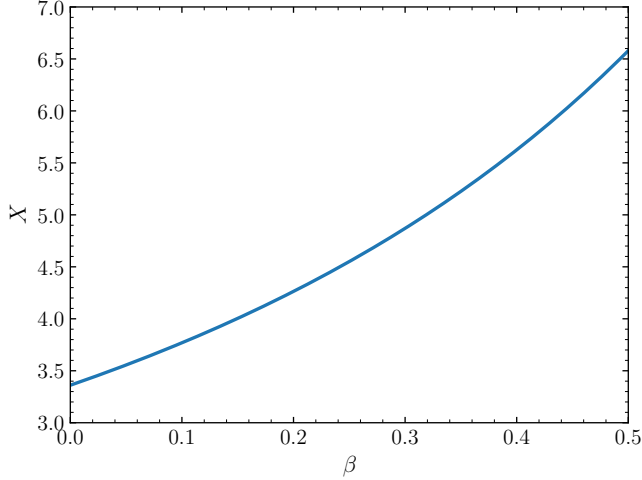


Figure 2. The ratio $X = R_{fil}/R_{\lambda}$ as a function of the wind parameter β (Eq. 6).

$z = 0.017175$. The SMBH is assumed to be a non-spinning Schwarzschild black hole. The inner and outer boundaries of the thin disk are $3 R_S$ and $2000 R_S$, respectively. The wind parameter is chosen to be $\beta = 0.3$; \dot{M}_0 is selected in such a way that $L_{bol} = 0.01 \dot{M}_{Edd} c^2$, where $\dot{M}_{Edd} = 10 L_{Edd}/c^2$ is the Eddington accretion rate (i.e., $L_{bol} = 0.1 L_{Edd}$).

This disk is illuminated with a driving light curve; the emission region of the driving light curve is assumed to be a point source located above the SMBH with a scale height of $H = 5 R_S$. It is argued that the observed X-ray light curves are not consistent with the driving light curve (Gardner & Done 2017; Starkey et al. 2017, but see Sun et al. 2018b). Therefore, we assume the driving light curve and the 1367 Å light curve are similar. The mean luminosity of the driving light curve ($L_{ill,u,0}$) is fixed to be 1/3 of the local viscous dissipation rate (Fausnaugh et al. 2016).

We fit the 1367 Å light curve with the *continuous time first-order autoregressive process* (i.e., CAR(1), whose PSD has the following shape $PSD(f) \propto 1/(f_0^2 + f^2)$, where f_0 is a characteristic frequency) via *CARMA*² (Kelly et al. 2014). We then generate mock light curves with a cadence of 0.1 day using *CARMA*. The baseline of a mock light curve is 180 days, which is similar to the observations of NGC 5548. The mock light curves heat the underlying accretion disk with time delays. The time lag is (Starkey et al. 2017)

$$\tau = \frac{\sqrt{H^2 + R^2} + H \cos i - R \cos \theta \sin i}{c}, \quad (7)$$

where θ is the azimuthal angle of the accretion disk. The temperature profile of the accretion disk is calculated at each epoch of the mock light curves. We can then obtain the mock light curves of different wavelengths by simply integrating the blackbody radiation over the whole disk. To ob-

² This package can be downloaded from <https://github.com/brandonckelly/carma.pack>.

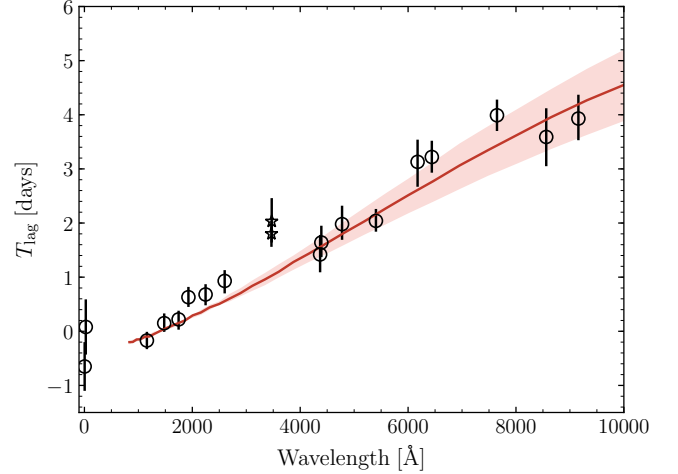


Figure 3. Time lag (with respect to the 1367 Å continuum) as a function of rest-frame wavelength for NGC 5548 (Edelson et al. 2015; Fausnaugh et al. 2016). The two star symbols denote the time lags of u and U bands; they are outliers since the two bands are significantly contaminated by BEL emission (Fausnaugh et al. 2016). The red solid curve indicates the time lag-wavelength relation for our model. The 1σ fluctuations (i.e., the shaded region) are derived from our 256 reprocessing simulations.

tain the time lags relative to the 1367 Å light curve as a function of wavelength, we adopt ICCFs (the interpolation cross-correlation function, which shows the correlation coefficient (ρ) as a function of time delay; see, e.g., Peterson et al. 1998).³ The time lags are estimated from the centroid of the ICCF, defined as the ρ -weighted lag for which $\rho > 0.8\rho_{max}$. We repeat this simulation 256 times.

In Figure 3, we show the time lag as a function of wavelength for our model. For UV-optical bands, the relation follows the $4/(3 - \beta)$ law (see Eq. 4); however, for near-IR bands, the relation is flatter because the outer boundary of the disk, which is fixed to $2000 R_S$, limits the time lags (i.e., Eq. 6 over-predicts X).⁴ Our model can explain the observed time lag-wavelength relation well.

We can calculate the spectral energy distribution (SED) of a disk that suffers from winds by simply integrating the blackbody emission of the temperature profile of Eq. 3 over the whole accretion disk. In Figure 4, we plot the luminosity density L_{ν} versus λ from our model (the blue dashed curve). While our model can fit the optical-IR emission well, it over-predicts the UV emission by a factor of ~ 2 . This inconsistency might be resolved in several ways. For instance, the intrinsic dust extinction can suppress UV emission. To illustrate this idea, we consider the Small Magel-

³ We use PYCCF, Python Cross Correlation Function for reverberation mapping studies, to calculate the ICCFs. For details, see <http://ascl.net/code/v/1868>.

⁴ It is unlikely that the outer boundary can be significantly larger than $2000 R_S$ since self gravity will truncate the accretion disk.

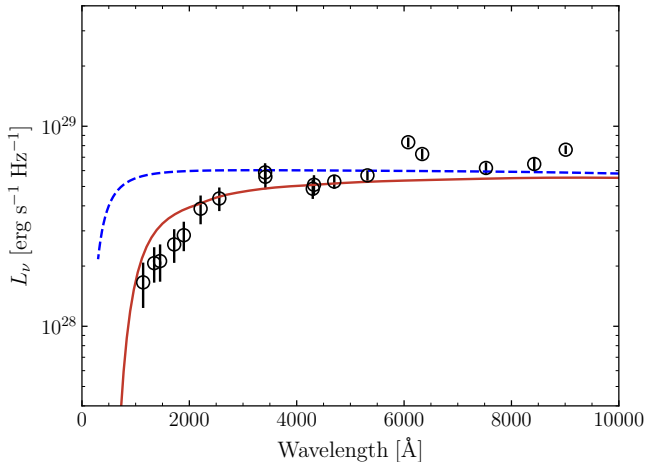


Figure 4. Broadband SED of NGC 5548 from Fausnaugh et al. (2016), which is corrected for Galactic extinction with a Milky Way extinction law (Cardelli et al. 1989) and $E(B - V) = 0.0171$ mag (Schlafly & Finkbeiner 2011). The blue dashed line indicates the SED of our disk-with-wind model. This SED over-predicts the observations in the short-wavelength end. However, such a discrepancy can be resolved if the SED suffers weak intrinsic extinction (for $E(B - V) = 0.05$ mag and the SMC extinction curve, the resulting SED is shown as the red solid curve).

lanic Cloud (SMC; Gordon et al. 2003) extinction curve with $E(B - V) = 0.05$ mag (Wamsteker et al. 1990). Under such extinction, the predicted SED (the red solid curve) can fit the UV-optical-IR data.

3. DISCUSSIONS

The observed larger-than-expected inter-band time lags indicate that some key ingredient is missing in the classical thin disk theory. We propose that the missing ingredient can be wind. If an AGN accretion disk suffers from strong winds, the temperature of the outer disk should be higher than the classical thin disk theory in order to produce the same bolometric luminosity and meanwhile the temperature profile is also flatter (see Figure 1). For a given band, the outer disk can contribute more to the observed flux. Therefore, our model can explain the observed larger-than-expected disk sizes (see Figures 2 & 3) as well as the observed UV-optical-IR SED (see Figure 4).

The disk-with-wind scenario has been proposed before to estimate the AGN mass growth rate and SED (Slone & Netzer 2012). Winds are expected from theoretical arguments (e.g., Blandford & Payne 1982; Jiao & Wu 2011; Cao & Spruit 2013; Gu 2015), numerical simulations (e.g., Ohsuga et al. 2009; Yuan et al. 2012a,b, 2015) and observational results (e.g., Weymann et al. 1991; Murray et al. 1995; Trump et al. 2006; Richards et al. 2011; Filiz Ak et al. 2014; Grier et al. 2015; Sun et al. 2018c). Such winds might be responsible for the observed warm absorbers in NGC 5548. In our model, the mass outflowing rate of the wind is $\sim 0.7 M_{\odot} \text{ yr}^{-1}$ (i.e., the difference of accretion rate between the inner and outer

boundaries), which is close to the observational implications ($\sim 0.3 M_{\odot} \text{ yr}^{-1}$; Ebrero et al. 2016). However, it is not realized until this work that the sizes of emission regions of such a disk are larger than those of the classical thin disk.

Our model can also be applied to other sources, such as NGC 4151 (Edelson et al. 2017), NGC 4593 (McHardy et al. 2017) or other ensemble studies (Jiang et al. 2017; Homayouni et al. in preparation). It also has the potential to reconcile microlensing observations of quasars with the classical thin accretion disk theory, which is detailed by Li et al. (in preparation).

In this work, we do not include a detailed discussion of the physics of winds. If our model is correct, we might use the observed disk sizes to infer wind strength β and test wind models. For instance, in the model of winds accelerated by the magnetic fields, $\beta \leq 1/3$ (Cao & Spruit 2013). However, β and \dot{M}_0 are degenerate. In this work, we fix $\beta = 0.3$ to explain the observations of NGC 5548. In principle, we can also assume a larger value of β (e.g., $\beta = 0.5$) and a smaller \dot{M}_0 to match the inter-band time lags of NGC 5548.

Our model is not the only one that can explain the observed time lag-wavelength relation of NGC 5548. Cai et al. (2018) propose a phenomenological model without X-ray reprocessing to explain the inter-band time lags. Meanwhile, Hall et al. (2018) suggest that, if the atmospheric density of an accretion disk is sufficiently low, scattering in the atmosphere can convert UV-optical photons into higher energy ones and produce apparently larger disk sizes. However, their model fails to match the UV-X-ray SED of NGC 5548. They also speculate that this inconsistency can be resolved if disk suffers from winds and the emission from the innermost regions is suppressed.

Our model cannot explain the large (i.e., a few days) time delay between hard X-ray and UV light curves. One possibility is that the observed time lag is contaminated by diffusion continuum emission from BEL region (McHardy et al. 2017; Sun et al. 2018b). It is also possible that the observed time delay does not correspond to the light-travel timescale but other timescales (e.g., the dynamical or thermal timescale of a UV torus; see, e.g., Edelson et al. 2017; Gardner & Done 2017).

All in all, our model can help decipher the UV-optical-IR time lags of current continuum reverberation mapping results. Future continuum reverberation mapping observations can test our model.

We thank J. X. Wang, F. Yuan and Z. Y. Cai for valuable discussions. M.Y.S. and Y.Q.X. acknowledge the support from NSFC-11603022, NSFC-11473026, NSFC-11421303, the 973 Program (2015CB857004), the China Postdoctoral Science Foundation (2016M600485), the CAS Frontier Science Key Research Program (QYZDJ-SSW-SLH006).

Software: Astropy (Astropy Collaboration et al. 2013), CARMA (Kelly et al. 2014), Matplotlib (Hunter 2007), Numpy & Scipy (Van Der Walt et al. 2011), PYCCF (Sun et al. 2018a)

REFERENCES

- Astropy Collaboration, Robitaille, T. P., Tollerud, E. J., et al. 2013, *A&A*, 558, A33
- Bentz, M. C., Walsh, J. L., Barth, A. J., et al. 2010, *ApJ*, 716, 993
- Blandford, R. D., & Payne, D. G. 1982, *MNRAS*, 199, 883
- Cackett, E. M., Chiang, C.-Y., McHardy, I., et al. 2017, arXiv:1712.04025
- Cackett, E. M., Horne, K., & Winkler, H. 2007, *MNRAS*, 380, 669
- Cai, Z.-Y., Wang, J.-X., Gu, W.-M., et al. 2016, *ApJ*, 826, 7
- Cai, Z.-Y., Wang, J.-X., Zhu, F.-F., et al. 2018, *ApJ*, 855, 117
- Cao, X., & Spruit, H. C. 2013, *ApJ*, 765, 149
- Cardelli, J. A., Clayton, G. C., & Mathis, J. S. 1989, *ApJ*, 345, 245
- Dexter, J., & Agol, E. 2011, *ApJL*, 727, L24
- Ebrero, J., Kaastra, J. S., Kriss, G. A., et al. 2016, *A&A*, 587, A129.
- Edelson, R., Gelbord, J., Cackett, E., et al. 2017, *ApJ*, 840, 41
- Edelson, R., Gelbord, J. M., Horne, K., et al. 2015, *ApJ*, 806, 129
- Fausnaugh, M. M., Denney, K. D., Barth, A. J., et al. 2016, *ApJ*, 821, 56
- Filiz Ak, N., Brandt, W. N., Hall, P. B., et al. 2014, *ApJ*, 791, 88
- Gardner, E., & Done, C. 2017, *MNRAS*, 470, 3591
- Gordon, K. D., Clayton, G. C., Misselt, K. A., Landolt, A. U., & Wolff, M. J. 2003, *ApJ*, 594, 279
- Grier, C. J., Hall, P. B., Brandt, W. N., et al. 2015, *ApJ*, 806, 111
- Gu, W.-M. 2015, *ApJ*, 799, 71
- Hall, P. B., Sarrouh, G. T., & Horne, K. 2018, *ApJ*, 854, 93
- Hunter, J. D. 2007, *Computing in Science and Engineering*, 9, 90
- Jiang, Y.-F., Green, P. J., Greene, J. E., et al. 2017, *ApJ*, 836, 186
- Jiao, C.-L., & Wu, X.-B. 2011, *ApJ*, 733, 112
- Kelly, B. C., Becker, A. C., Sobolewska, M., Siemiginowska, A., & Uttley, P. 2014, *ApJ*, 788, 33
- Krolik, J. H., Horne, K., Kallman, T. R., et al. 1991, *ApJ*, 371, 541
- McHardy, I., Connolly, S., Cackett, K. E., et al. 2017, arXiv:1712.04852
- Morgan, C. W., Kochanek, C. S., Morgan, N. D., & Falco, E. E. 2010, *ApJ*, 712, 1129
- Murray, N., Chiang, J., Grossman, S. A., & Voit, G. M. 1995, *ApJ*, 451, 498
- Ohsuga, K., Mineshige, S., Mori, M., & Kato, Y. 2009, *PASJ*, 61, L7
- Peterson, B. M., Wanders, I., Horne, K., et al. 1998, *PASP*, 110, 660
- Richards, G. T., Kruczek, N. E., Gallagher, S. C., et al. 2011, *AJ*, 141, 167
- Schlafly, E. F., & Finkbeiner, D. P. 2011, *ApJ*, 737, 103
- Shakura, N. I., & Sunyaev, R. A. 1973, *A&A*, 24, 337
- Slone, O., & Netzer, H. 2012, *MNRAS*, 426, 656
- Starkey, D., Horne, K., Fausnaugh, M. M., et al. 2017, *ApJ*, 835, 965
- Sun, M., Grier, C. J., Peterson, B. M. 2018a, *PYCCF, Astrophysics Source Code Library*, record ascl:1805.032
- Sun, M., Xue, Y., Cai, Z., & Guo, H. 2018b, *ApJ*, 857, 86
- Sun, M., Xue, Y., Richards, G. T., et al. 2018c, *ApJ*, 854, 128
- Trump, J. R., Hall, P. B., Reichard, T. A., et al. 2006, *ApJS*, 165, 1
- Van Der Walt, S., Colbert, S. C., & Varoquaux, G. 2011, arXiv:1102.1523
- Wamsteker, W., Rodriguez-Pascual, P., Wills, B. J., et al. 1990, *ApJ*, 354, 446
- Weymann, R. J., Morris, S. L., Foltz, C. B., & Hewett, P. C. 1991, *ApJ*, 373, 23
- Yuan, F., Wu, M., & Bu, D. 2012a, *ApJ*, 761, 129
- Yuan, F., Bu, D., & Wu, M. 2012b, *ApJ*, 761, 130
- Yuan, F., Gan, Z., Narayan, R., et al. 2015, *ApJ*, 804, 101
- Zhu, F.-F., Wang, J.-X., Cai, Z.-Y., et al. 2018, *ApJ*, in press (arXiv:1711.00870)